Space group theory and Fourier space analysis of two-dimensional photonic crystal waveguides

Adam Mock*
School of Engineering and Technology, Central Michigan University, Mt. Pleasant, Michigan 48859, USA

Ling Lu and John O'Brien
Electrical Engineering Department, University of Southern California, Los Angeles, California 90089, USA

(Received 15 December 2009; revised manuscript received 26 March 2010; published 19 April 2010)

The symmetry, Fourier space and space group properties of two-dimensional photonic crystal waveguides are discussed. The modes of the standard single missing line defect waveguide can be classified as even or odd along the transverse direction. This is contrasted with the modes of line defect waveguides with a glide plane along the propagation direction. In this case the spatial Fourier series components of a single mode alternate between even and odd. The theory of symmorphic and nonsymmorphic space groups is used to classify the modes of these two waveguides, and the pairwise degeneracy at the Brillouin zone boundary is predicted for the waveguide with a glide-plane. Three-dimensional finite-difference time-domain numerical calculations are used to illustrate the investigated symmetry properties.

DOI: 10.1103/PhysRevB.81.155115 PACS number(s): 42.70.Qs, 78.67.Pt, 42.82.Et

I. INTRODUCTION

Two-dimensional photonic crystal geometries patterned in finite-height dielectric or semiconductor slabs have been the focus of significant research recently.[1–5] The optical modes are confined vertically via index guiding and the in-plane properties are defined by the photonic crystal hole pattern. The introduction of defects into the periodic lattice has allowed control of the direction[6] and speed[7] of light propagation. Furthermore it has been shown that two-dimensional photonic crystal resonant cavities exhibit large quality (Q) factors with mode volumes on the order of a cubic wavelength.[8,9] Two-dimensional photonic crystal slab waveguides are important building blocks for photonic integrated circuits due to their compact size, lithographic tunability, and low bending-loss. The two-dimensional patterning makes photonic crystal devices compatible with the layer-by-layer fabrication process for planer lightwave circuits. They are also attractive for generating slow light and enhancing light-matter interactions.

Much of the progress in designing low loss waveguides and large Q factor cavities has been carried out utilizing a free-standing suspended dielectric or semiconductor membrane, so that the index contrast between the dielectric slab and the top and bottom cladding is maximized. For photonic crystal waveguides, this maximizes the low-loss transmission bandwidth which is bounded by the light line for short wavelengths and the photonic crystal waveguide band edge at long wavelengths.[10] For photonic crystal cavities, the light-cone projection onto the two-dimensional spatial Fourier transform of the resonant mode is minimized when the top and bottom cladding is air. This reduces the number of wavevector components radiating out-of-plane[11] and has allowed for Q factors exceeding one million.[9,12]

Although many suspended membrane devices have been successfully demonstrated due to low out-of-plane optical loss, there is significant motivation for including dielectric or semiconductor top and bottom cladding layers for building technologically viable devices. These advantages include improved vertical heat dissipation, improved electrical conductivity and better mechanical stability. These improvements come at the cost of lower vertical index contrast, which reduces the low-loss waveguide bandwidth[13] and decreases the cavity Q factor.[14]

One approach to reducing the out-of-plane losses of photonic crystal waveguides when the vertical index contrast is reduced is through the introduction of a glide plane along the waveguide propagation direction. As will be discussed later, the addition of a glide plane to the photonic crystal waveguide introduces nonsymmorphic space group symmetry. This configuration has been termed type B to differentiate it from a line defect waveguide which we will refer to as type A.[15,16] Schematic diagrams of type A and type B photonic crystal waveguides are shown in Figure 1. The type B waveguide is formed from a type A waveguide by shifting one side of the photonic crystal cladding by one half lattice constant along the x direction. Numerical calculations predict that radiation losses for modes above the light line in a type B waveguide can be as much as two orders of magnitude lower than that of a type A waveguide.[16]

The reduced out-of-plane optical losses associated with the type B waveguide have also been utilized in the design of resonant cavities that include a dielectric lower substrate for improved heat dissipation.[17,18] These studies were motivated by the goal of achieving continuous wave photonic crystal laser operation. The photonic crystal double heterostructure cavity was featured in these studies and is formed by perturbing a few periods of an otherwise straight waveguide. When the heterostructure is formed from a type A waveguide in a suspended membrane, it has been shown to have a Q factor in excess of 10^6 with a mode volume on the order of a cubic wavelength.[9,12] However, the Q factor is significantly reduced as the vertical index contrast is lowered. Forming the heterostructure in a type B waveguide has resulted in an improvement in the Q factor by as much as a factor of 5 when the index of the lower cladding is in the range of 1.4 to 1.8.[18]

In this work, we explore the modal and band-structure properties of photonic crystal waveguides and focus on the interesting effects of the nonsymmorphic space group sym-

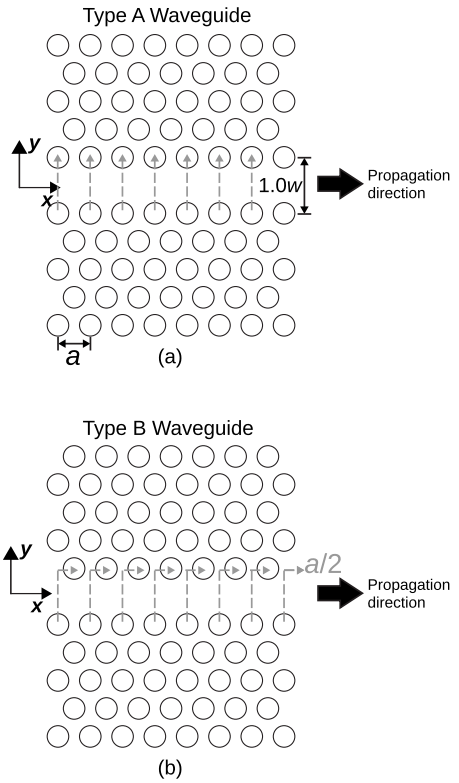

FIG. 1. Schematic depiction of single missing line defect photonic crystal waveguides. $w=\sqrt{3}a$ corresponds to the distance associated with a single missing line defect. a is the photonic crystal lattice constant and is illustrated in (a). (a) Type A waveguide in which the photonic crystal lattice on each side of the waveguide core is aligned. (b) Type B waveguide in which the photonic crystal lattice on each side of the core is shifted along x by $a/2$.

metry on the modes of the type B waveguide. Specifically we show that the bands associated with a type A waveguide can be classified as either even or odd along the y direction whereas for a type B waveguide, the bands are neither even nor odd but exist as pairs with closely related symmetry properties. The modes of type A and type B waveguides are characterized formally using space group theory. The frequencies of the paired type B waveguide bands become degenerate at the Brillouin zone boundary and we derive this result using the group theory of nonsymmorphic space groups and provide a physical explanation of its origin. In addition to its general theoretical interest, this work has direct application in the design of photonic crystal heterostructure cavities,[18] the design of waveguide bends[19] and waveguide band-structure engineering in general.[7] Similar lattice shifting approaches have been employed to increase the slow light bandwidth in photonic crystal waveguides.[20] Because its waveguide bands flatten and become pairwise degenerate at the Brillouin zone edge boundary, the type B waveguide could potentially double the slow light bandwidth of photonic crystal waveguides.

II. COMPUTATIONAL METHOD

Figure 2 shows the evolution of the photonic crystal

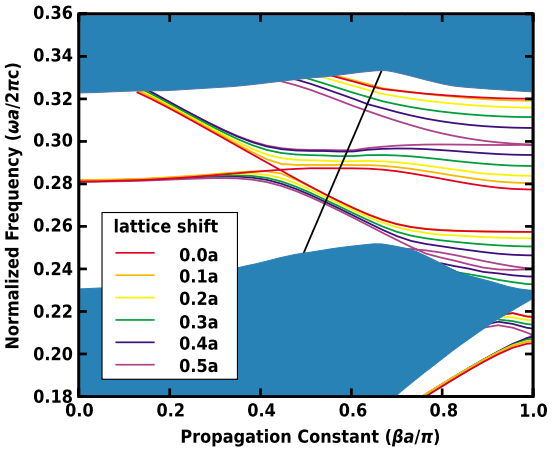

FIG. 2. (Color online) Photonic crystal waveguide dispersion diagram for six different photonic crystal waveguides. A lattice shift of $0.0a$ corresponds to a type A waveguide. The photonic crystal lattice on the two sides of the waveguide core are shifted along the x direction until $0.5a$ which corresponds to a type B waveguide. The solid portions of the plot depict the projection of the photonic crystal cladding modes onto the waveguide dispersion diagram. The straight line cutting diagonally across the diagram is the light line. The vertical axis is normalized frequency, where c is the vacuum speed of light.

waveguide band structure as one side of the photonic crystal lattice is shifted along the waveguide propagation direction. The initial configuration without any shift corresponds to a type A waveguide and the final configuration with a $0.5a$ (where a is the lattice constant) shift corresponds to the type B waveguide. The structure analyzed in Fig. 2 consists of a free-standing semiconductor membrane with a refractive index of $n=3.505$ consistent with silicon at a wavelength of 1.5 μm. The silicon membrane thickness to lattice constant ratio was set to $d/a=0.6$. The hole radius to lattice constant ratio was set to $r/a=0.30$. The waveguide and photonic crystal modes depicted in Fig. 2 are the lowest frequency modes corresponding to the transverse electric polarization (H_z is even in the z direction).

The band structure was calculated using the finite-difference time-domain method.[21] Because of the periodicity of the structure, only a single unit cell of the waveguide was analyzed, and Bloch boundary conditions along the propagation direction (x direction in Fig. 1) were used to simulate an infinite structure.[13] Perfectly matched layer absorbing boundary conditions were used to terminate the other boundaries. The structure was discretized using 20 points per lattice constant. The total domain included $20\times340\times200$ discretization points along the (x,y,z) directions. The blue shaded regions correspond to the projection of the photonic crystal cladding modes. These modes were also calculated using the finite-difference time-domain method with Bloch boundary conditions.[22] In order to generate the band structure in Fig. 2, simulations were run for individual β values spanning the first Brillouin zone from $\beta=0$ to $\beta=\pi/a$. For each β, a broad band initial condition was used to generate a 2×10^5 element time sequence. The time sequences were discrete Fourier transformed, and Padé (Ref. 23) interpolation was used to estimate the center frequency.

III. BANDSTRUCTURE DISCUSSION

A. Qualitative properties of type A and type B waveguide bands

Figure 2 displays the waveguide dispersion bands for six different waveguides. The curves labeled $0.0a$ represent the dispersion of the standard type A waveguide in which the photonic crystal cladding making up the two sides of the waveguide have not been shifted. The curves labeled $0.5a$ correspond to the dispersion of the type B waveguide in which the photonic crystal cladding making up the two sides of the waveguide have been shifted by one half lattice constant. The remaining curves correspond to the dispersion of waveguides with varying degrees of lattice shift and illustrate how the dispersion bands of the type A waveguide evolve into those of the type B waveguide.

One striking feature of Fig. 2 is the transition from a band crossing for the type A structure to a band anticrossing for every other waveguide near $\beta a/\pi=0.44$. In general, modes associated with different bands (labeled by n_i) in a photonic crystal waveguide are orthogonal, and modes associated with the same band but at different propagation constants are orthogonal: $\int \epsilon(\vec{r})\vec{E}_{n_1}^{\beta_1}(\vec{r})\cdot\vec{E}_{n_2}^{\beta_2*}(\vec{r})d^3\vec{r}=\delta(\beta_1-\beta_2)\delta_{n_1,n_2}$. This indicates that the two bands that either cross or anticross at $\beta a/\pi=0.44$ have three-dimensional field distributions whose overlap integrals equate to zero: $\int \epsilon(\vec{r})\vec{E}_{n_1}^{\beta}(\vec{r})\cdot\vec{E}_{n_2}^{\beta*}(\vec{r})d^3\vec{r}=0$. If we consider the shifting of one side of the photonic crystal lattice to be a perturbation to the unshifted type A waveguide, coupled mode theory tells us that the coupling constants characterizing the interaction between waveguide modes involve spatial overlap integrals of the form

$$\kappa \propto \int \vec{E}_{n_1}^{\beta}(\vec{r})\cdot\vec{E}_{n_2}^{\beta*}(\vec{r})[\epsilon_A(x,y,z)+\Delta\epsilon(x,y,z)]d^3\vec{r}, \qquad (1)$$

where $\vec{E}_{n_i}^{\beta}(\vec{r})=\vec{E}_{n_i}^{\beta}(x,y,z)$ is the electric field of a type A waveguide mode labeled by $i=\{1,2\}$, $\epsilon_A(x,y,z)$ represents the dielectric distribution of the type A waveguide and $\Delta\epsilon(x,y,z)=\epsilon(x,y,z)-\epsilon_A(x,y,z)$ represents deviation from the type A waveguide structure induced by the photonic crystal lattice shift. For the type A waveguide, $\Delta\epsilon(x,y,z)=0$ and $\epsilon_A(x,y,z)=\epsilon_A(x,-y,z)$ which suggests that the $\vec{E}_{n_i}^{\beta}(x,y,z)$ is either even or odd along the y direction. If $\vec{E}_{n_1}^{\beta}(x,y,z)$ is odd and $\vec{E}_{n_2}(x,y,z)$ is even along the y direciton (or vice versa) and $\epsilon(x,y,z)$ is even, κ vanishes, and there is no coupling between the bands associated with $\vec{E}_{n_1}^{\beta}$ and $\vec{E}_{n_2}^{\beta}$. Previous studies of the spatial modes associated with the two bands that cross for the type A waveguide have shown that one mode is odd and one mode is even along the y direction.[10] This results in $\kappa=0$ for the two type A waveguide modes at $\beta a/\pi=0.44$, and crossing is allowed. When one side of the photonic crystal lattice is shifted, $\Delta\epsilon(x,y,z)\neq 0$ and $\Delta\epsilon(x,y,z)\neq\Delta\epsilon(x,-y,z)$. If κ is evaluated using the unperturbed even and odd modes of the type A waveguide, then $\kappa\neq 0$, which causes the modes to anticross. This argument provides a qualitative explanation of why the type A waveguide bands cross at $\beta a/\pi=0.44$, and bands associated with lattice shifted geometries anticross.

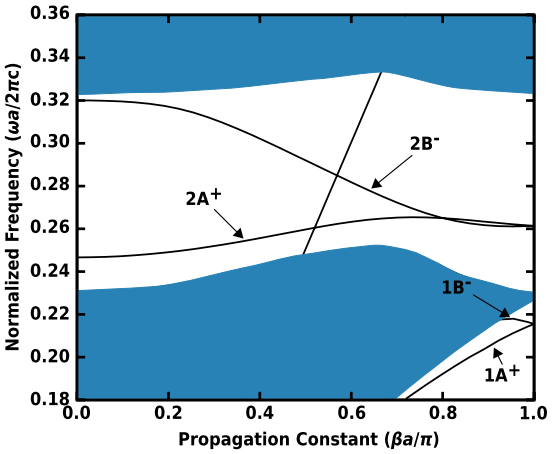

FIG. 3. (Color online) Photonic crystal waveguide dispersion diagram for a type B waveguide with a waveguide core thickness of $0.8w$ where w is defined in Fig. 1.

Another interesting feature displayed in Fig. 2 is the evolution toward pairwise degeneracy of the waveguide bands at the Brillouin zone boundary $\beta=\pi/a$ as the structure evolves from a type A to a B waveguide. In addition to its theoretical interest, understanding this degeneracy is particularly important for the design of heterostructure cavities, as the heterostructure bound state resonances form near waveguide dispersion extrema which often occur near the Brillouin zone boundary.[24] Constructing a heterostructure cavity from a type B waveguide results in a cavity with two closely spaced resonant modes as a result of this band degeneracy. In what follows we investigate the y-direction symmetry of the type B waveguide bands, and we find that for the bands considered in Fig. 2, the two bands that become degenerate at $\beta=\pi/a$ have different but related y-direction symmetry. With this understanding one may modify the type B waveguide in order to control the behavior of these modes in order to improve device performance for a particular application.

Before proceeding with the analysis, we present a waveguide band-structure dispersion diagram shown in Fig. 3 for a type B waveguide with a reduced waveguide core width of $0.8w$ (see Fig. 1). In Fig. 2, the lowest frequency waveguide band inside the photonic crystal bandgap for a type B waveguide partly overlaps with the low-frequency photonic crystal modes. By reducing the photonic crystal waveguide core width, one changes the effective index of the mode and thus tunes the waveguide modes.[10] In Fig. 3, the lowest-frequency modes inside the band gap have been shifted to higher frequencies toward the middle of the band gap. The purpose of this tuning is to clarify the shape of these two waveguide bands by allowing them to span the entire Brillouin zone. It will also make obtaining the field profiles for an arbitrary β value more straight forward which we do at the end of this section. It should be noted that reducing the waveguide core width does not change the transverse symmetry of the waveguide. The type A and B labels still apply, and the type B waveguide is still characterized by a glide plane. The space group theory labels discussed in Sec. IV apply to waveguide structures with arbitrary core widths. When the photonic crystal waveguide core width is tuned (either larger or

smaller), the waveguide is no longer associated with a simple missing line defect. However, this does not have any consequences in the present discussion. It is also interesting to note that this reduced width tuning is beneficial for device applications. The reduced width type B waveguide has a larger bandwidth (beneficial for wavelength division multiplexed telecommunication applications) and smaller mode volume (beneficial for lowering power and nonlinear applications).

B. Fourier space properties of type A and type B waveguide modes

In this subsection we use the Bloch-mode properties of photonic crystal waveguide modes to uncover the modal properties of type A and type B waveguides. In particular we derive a Fourier space relationship between the two modes that become degenerate at the Brillouin zone boundary in the type B waveguide. We begin by writing the real-space distribution of a particular waveguide mode according to Bloch's theorem

$$F_i(x,y,z) = u_{i,\beta}(x,y,z)e^{-i\beta x}. \tag{2}$$

In Eq. (2), $F_i(x,y,z)$ is the ith field component, and $u_{i,\beta}(x+a,y,z)=u_{i,\beta}(x,y,z)$ is periodic along the propagation direction (x). The z dependence of $u_{i,\beta}(x,y,z)$ is similar to that of the fundamental slab mode, and the y dependence is consistent with the confinement behavior of a photonic crystal waveguide along the y direction. Because $u_\beta(x,y,z)$ (we suppress the subscript i from here on to simplify notation) is periodic along x, it can be written as a Fourier series

$$u_\beta(x,y,z) = \sum_{n=-\infty}^{n=+\infty} f_n^\beta(y,z)e^{-ix(2\pi/a)n}, \tag{3}$$

where $f_n^\beta(y,z)$ is the nth spatial Fourier series component of the mode with propagation constant β. So any photonic crystal waveguide mode can be expressed as

$$F(x,y,z) = \sum_{n=-\infty}^{n=+\infty} f_n^\beta(y,z)e^{-ix(\beta+(2\pi/a)n)}. \tag{4}$$

First we consider a type A photonic crystal waveguide in which the structure is invariant under a mirror operation about the x axis, $\hat{\sigma}_y$, which takes y to $-y$. Because of this invariance, we expect the field solutions to be eigenfunctions of this operator with eigenvalue σ_y: $\hat{\sigma}_y F(x,y,z) = \sigma_y F(x,y,z)$. Because applying σ_y twice returns a field component to its original configuration, one gets $\hat{\sigma}_y\hat{\sigma}_y=\hat{1}$, where $\hat{1}$ is the identity operator. Subsequently one has $\hat{\sigma}_y\hat{\sigma}_y F(x,y,z)=\sigma_y^2 F(x,y,z)=\hat{1}F(x,y,z)$ resulting in $\sigma_y=\pm 1$. Therefore $\hat{\sigma}_y F(x,y,z)=F(x,-y,z)=\pm F(x,y,z)$ showing that the type A waveguide modes will be either even or odd along the y direction about the center of the waveguide. For the type A waveguide band structure in Fig. 2, $H_z(x,y,z)$ corresponding to the lowest-frequency band in the bandgap is even about $y=0$, and $H_z(x,y,z)$ corresponding to the second lowest frequency band in the band gap is odd about $y=0$. (A more complete labeling of the modes is given in Fig. 9.) In terms of the Fourier series expansion of these modes, the even/odd symmetry along y results in

$$\begin{aligned}\hat{\sigma}_y F(x,y,z) &= F(x,-y,z)\\ &= \sum_{n=-\infty}^{n=+\infty} f_n^\beta(-y,z)e^{-ix(\beta+(2\pi/a)n)}\\ &= \pm F(x,y,z)\\ &= \pm \sum_{n=-\infty}^{n=+\infty} f_n^\beta(y,z)e^{-ix(\beta+(2\pi/a)n)}.\end{aligned} \tag{5}$$

Comparing the second and fourth lines implies $f_n^\beta(-y,z)=\pm f_n^\beta(y,z)$. This means that for a mode with even (odd) symmetry along the y direction, every spatial Fourier series component of that mode will also have even (odd) symmetry along the y direction.

For the type B waveguide, the structure is no longer invariant under $\hat{\sigma}_y$, and the modes cannot be classified as either even or odd along the y direction. However, the waveguide is invariant under $\hat{\sigma}_y$ followed by a translation along the x direction by one half lattice constant, $\hat{T}_x(a/2)$. This type of operation is known as glide reflection, and the glide reflection plane (or glide plane) is described by $y=0$. To simplify notation, we define the operator $\hat{g}=\hat{\sigma}_y\hat{T}_x(a/2)$. Again, due to the invariance of the structure under $\hat{g}$, we expect the field solutions to be eigenfunctions of this operator with eigenvalues g: $\hat{g}F(x,y,z)=gF(x,y,z)$. Application of $\hat{g}$ twice results in a translation along the x direction by a. From Bloch's theorem, one has $\hat{g}\hat{g}F(x,y,z)=F(x+a,y,z)=e^{-i\beta a}F(x,y,z)$. Therefore, the eigenvalues of the operator $\hat{g}$ operating on a field component $F(x,y,z)$ are $g=\pm e^{-i\beta a/2}$.

In terms of the Fourier series expansion of these modes, application of $\hat{g}$ results in

$$\begin{aligned}\hat{g}F(x,y,z) &= \sum_{n=-\infty}^{n=+\infty} f_n^\beta(-y,z)e^{-i(x+a/2)(\beta+(2\pi/a)n)}\\ &= e^{-i\beta a/2}\sum_{n=-\infty}^{n=+\infty} e^{-i\pi n} f_n^\beta(-y,z)e^{-ix(\beta+(2\pi/a)n)}\\ &= \pm e^{-i\beta a/2}F(x,y,z)\\ &= \pm e^{-i\beta a/2}\sum_{n=-\infty}^{n=+\infty} f_n^\beta(y,z)e^{-ix(\beta+(2\pi/a)n)}.\end{aligned} \tag{6}$$

Comparing the second and fourth lines shows that the Fourier components of the type B waveguide modes have the following property

$$e^{-i\pi n} f_n^\beta(-y,z) = \pm f_n^\beta(y,z). \tag{7}$$

As stated earlier, the waveguide modes of the type B waveguide are not simply even or odd along the y direction. Equation (7) illustrates that they are made up of Fourier series components that *alternate* between even and odd symmetry along the y direction. This concept is illustrated in Table I which lists the results of Eq. (7) for Fourier series components labeled by indicies $n=\{\ldots -2,-1,0,1,2,\ldots\}$. The modes of the type B waveguide will behave according to

TABLE I. Symmetry of spatial Fourier series components according to Eq. (7).

n	$+(1A^+,2A^+)$	$-(1B^-,2B^-)$
−2	$f^{\beta}_{-2}(-y,z)=f^{\beta}_{-2}(y,z)$ even	$f^{\beta}_{-2}(-y,z)=-f^{\beta}_{-2}(y,z)$ odd
−1	$-f^{\beta}_{-1}(-y,z)=f^{\beta}_{1}(y,z)$ odd	$-f^{\beta}_{-1}(-y,z)=-f^{\beta}_{-1}(y,z)$ even
0	$f^{\beta}_{0}(-y,z)=f^{\beta}_{0}(y,z)$ even	$f^{\beta}_{0}(-y,z)=-f^{\beta}_{0}(y,z)$ odd
1	$-f^{\beta}_{1}(-y,z)=f^{\beta}_{1}(y,z)$ odd	$-f^{\beta}_{1}(-y,z)=-f^{\beta}_{1}(y,z)$ even
2	$f^{\beta}_{2}(-y,z)=f^{\beta}_{2}(y,z)$ even	$f^{\beta}_{2}(-y,z)=-f^{\beta}_{2}(y,z)$ odd

either the second (labeled by "+") or the third (labeled by "−") column of Table I. For the + modes, the Fourier component in the first Fourier space unit cell is even, the Fourier components in the second Fourier space unit cell ($n=\pm 1$) are odd, the Fourier components in the third Fourier space unit cell ($n=\pm 2$) are even, and so on. The first Fourier space unit cell refers to the region $-\pi/a<\beta<\pi/a$. The second Fourier space unit cell refers to the regions $\pi/a<\beta<3\pi/a$ and $-3\pi/a<\beta<-\pi/a$. The third Fourier space unit cell refers to the regions $3\pi/a<\beta<5\pi/a$ and $-5\pi/a<\beta<-3\pi/a$. A similar situation is true for the − modes: the Fourier component in the first Fourier space unit cell ($n=0$) is odd, the Fourier components in the second Fourier space unit cell ($n=\pm 1$) are even, the Fourier components in the third Fourier space unit cell ($n=\pm 2$) are odd, and so on.

C. Illustration of symmetry properties in field profiles

In this subsection we illustrate the symmetry property [Eq. (7)] associated with the type B waveguide modes that was derived in the previous subsection. Fig. 4 illustrates the $H_z(x,y,z=0)$ field profiles associated with the modes labeled $2A^+$ and $2B^-$ in Fig. 3 for $\beta a=2.0=0.634\pi$. $z=0$ corresponds to the midplane of the slab where the H_z component is completely scalar for the TE-like slab mode. From Fig. 4 it is clear that these modes are neither even nor odd about y. Qualitatively speaking, the modes appear to "zigzag" along the waveguide core as a result of the photonic crystal lattice being a half lattice period out of phase on either side of the core. It is also interesting to note that the mode associated with the band labeled $2A^+$ in Fig. 3 has weaker confinement along the y direction than that of mode $2B^-$. This is due to the small frequency spacing between the $2A^+$ waveguide mode and the low frequency band associated with the photonic crystal cladding modes. That is, mode $2A^+$ is weakly confined by the photonic crystal lattice due to its shallow placement in the band gap.

In Figs. 5(a) and 6(a) we display the spatial Fourier transform of the modes depicted in Figs. 4(a) and 4(b), respectively. The spatial Fourier transforms consist of a series of discrete peaks along the β direction. Each peak has a continuous distribution along k_y. These peaks correspond to the

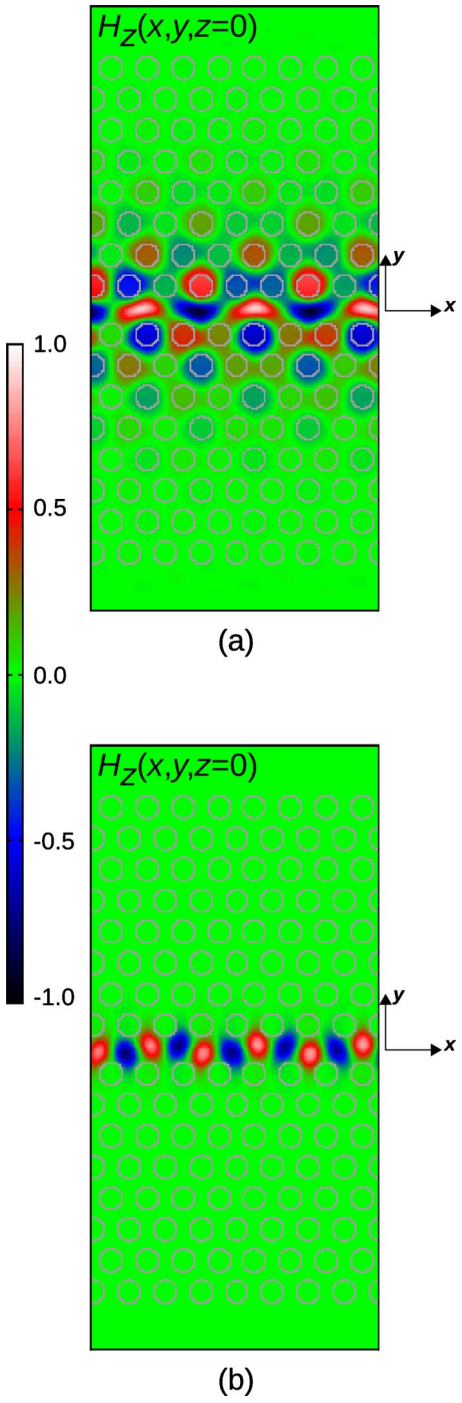

FIG. 4. (Color online) $H_z(x,y,z=0)$ field distribution for the modes labeled (a) $2A^+$ and (b) $2B^-$ in Fig. 3 corresponding to a propagation constant of $\beta=2.0/a$.

Fourier series components in Eq. (4). Ideally these peaks should be delta functions along the β direction with zero width. The finite width of the peaks shown in Figs. 5 and 6 is due to the finite spectral width filtering operation used to isolate these modes in our finite-difference time-domain simulation. It should be noted that Fourier space distributions are plotted on a logarithmic scale indicating that the Fourier peaks at $\beta=2.0/a+n2\pi/a$ (where n is an integer) are several

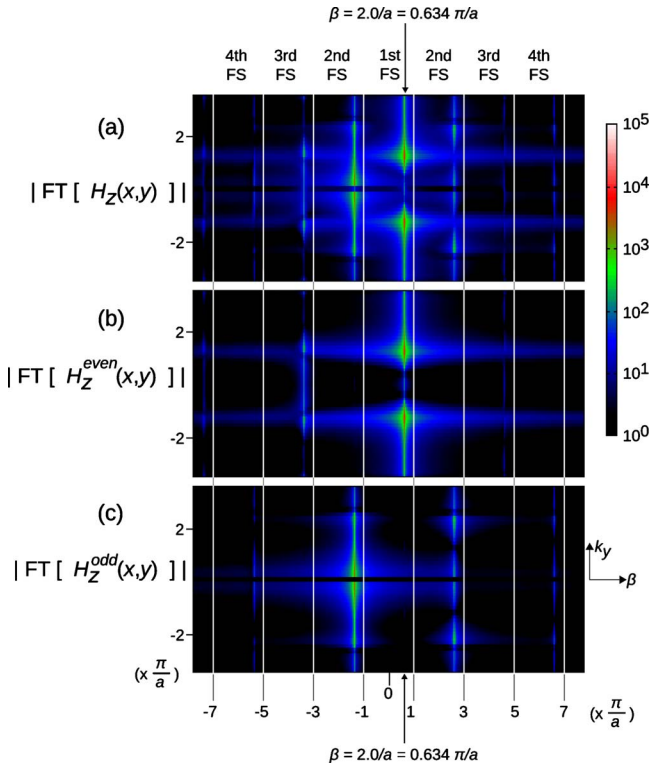

FIG. 5. (Color online) (a) Spatial Fourier transform of the mode shown in Fig. 4(a). At the bottom are spatial Fourier transforms for the even (b) and odd (c) components of $H_z(x,y,z=0)$. FS and FT stand for Fourier space unit cell and Fourier transform, respectively.

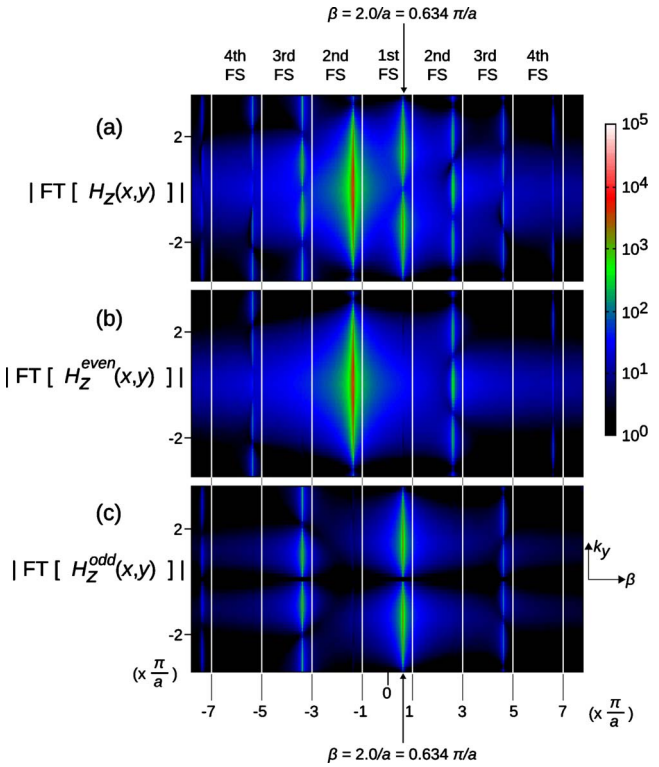

FIG. 6. (Color online) (a) Spatial Fourier transform of the mode shown in Fig. 4(b). At the bottom are spatial Fourier transforms for the even (b) and odd (c) components of $H_z(x,y,z=0)$. FS and FT stand for Fourier space unit cell and Fourier transform, respectively.

orders of magnitude larger than elsewhere in the Fourier space plot.

As stated earlier, these modes have a propagation constant $\beta=2.0/a$. It is clear that for both modes, the highest amplitude Fourier series component $[f_n^{\beta}(k_y,z=0)]$ is in the first Fourier space unit cell $[f_0^{\beta}(k_y,z=0)]$ and is labeled in Figs. 5 and 6. The Fourier series peaks are separated in Fourier space along the β direction by the reciprocal lattice vectors of the waveguide, which point along the β direction and have magnitude $2\pi/a$. It is also apparent that the amplitude of the Fourier series peaks decreases as one moves away from the first Brillouin zone.

Just below the spatial Fourier transforms in the top portions of Figs. 5 and 6, we have plotted the spatial Fourier transforms of $H_z^{even}(x,y,z=0)$ and $H_z^{odd}(x,y,z=0)$. $H_z^{even}(x,y,z=0)=\frac{1}{2}[H_z(x,y,z=0)+H_z(x,-y,z=0)]$ and $H_z^{odd}(x,y,z=0)=\frac{1}{2}[H_z(x,y,z=0)-H_z(x,-y,z=0)]$. Note that the Fourier space distribution for $H_z^{odd}(x,y,z=0)$ passes through zero at $k_y=0$. This results in the dark line along $k_y=0$ in Fig. 5(c) and 6(c) (its thickness and abruptness is due to the limited resolution in the k_y direction).

H_z^{even} and H_z^{odd} represent the decomposition of H_z into its even and odd (along y) components. From Fig. 5 we see that the Fourier series components making up the even component of the mode are located in the first and third Fourier space unit cells, and the Fourier series components making up the odd component of the mode are located in the second and fourth Fourier space unit cells. Comparison to the results of Table I, shows that the mode labeled $2A^+$ in Fig. 3 has the characteristics of the eigenfunction associated with the + sign (hence the + label already in place) implying its eigenvalue under $\hat{g}$ is $g=+e^{-i\beta a/2}$.

In Fig. 6, we plot the spatial Fourier transform for the mode labeled $2B^-$ in Fig. 3. In this case, we see that the Fourier series components making up the even component of the mode are located in the second and fourth Fourier space unit cells, and the Fourier series components making up the odd component of the mode are located in the first and third Fourier space unit cells. Comparison to the results of Table I, shows that the mode labeled $2B^-$ in Fig. 3 has the characteristics of the eigenfunction associated with the − sign (hence the − label already in place) implying its eigenvalue under $\hat{g}$ is $g=-e^{-i\beta a/2}$.

We have also analyzed the symmetry properties of the modes labeled $1A^+$ and $1B^-$ in Fig. 3. The mode labeled $1A^+$ transforms according to the + sign in Eq. (7) and the mode labeled $1B^-$ transforms according to the − sign. For the two sets of bands shown in Fig. 3, one sees that for the two bands that become degenerate at the Brillouin zone boundary, one will have y-direction symmetry defined by the + sign in Eq. (7), and the other will have y-direction symmetry defined by the − sign.

Careful inspection of Figs. 5(b) and 5(c) reveal that small Fourier series peak remain in the second Fourier space unit cell of the spatial Fourier transform of $H_z^{even}(x,y,z=0)$ and in the first and third Fourier space unit cells of $H_z^{odd}(x,y,z=0)$. Similarly, careful inspection of Figs. 6(b) and 6(c) reveal that small Fourier series peaks remain in the

TABLE II. Character table of C_{2v} point group.

$C_{2v}(2mm)$	E	C_2	σ_x	σ_y
A_1	1	1	1	1
A_2	1	1	−1	−1
B_1	1	−1	1	−1
B_2	1	−1	−1	1

first and third Fourier space unit cells of the spatial Fourier transform of $H_z^{even}(x,y,z=0)$ and in the second Fourier space unit cell of $H_z^{odd}(x,y,z=0)$. These peaks are numerical artifacts resulting from the limited sidelobe suppression in our discrete-time filtering window.[25] Some residual amplitude corresponding to mode $2A^+$ remains in Fig. 6, and some residual amplitude corresponding to mode $2B^-$ remains in Fig. 5. Our Blackman window is expected to provide about 60 dB of suppression outside of the main filter lobe, and the residual peaks appearing in Figs. 5(b), 5(c), 6(b), and 6(c) have been suppressed by approximately this amount. Despite this issue, the symmetry relation implied by Eq. (7) is clearly illustrated in Figs. 5 and 6.

D. Understanding the pairwise degeneracy of type B waveguides

In this section, we provide some physical insight into the pairwise degeneracy at the Brillouin zone boundary for the Type B waveguide. Due to the time reversability of Maxwell's equations, waveguide modes are unchanged if the sign of the propagation constant is changed as $\beta \rightarrow -\beta$. When the transformation $\beta \rightarrow -\beta$ is applied, the original mode is obtained by taking $t \rightarrow -t$, where t is time. This allows one to plot only positive values of β in waveguide dispersion relations: the dispersion relation can be mirrored about $\beta=0$ to obtain the relation for the negative β values.

As $\beta \rightarrow \pi/a$, Fig. 5 suggests that mode $2A^+$ will have even Fourier series components at $\beta=\{\ldots,-3\frac{\pi}{a},1\frac{\pi}{a},5\frac{\pi}{a},\ldots\}$. Similarly, Fig. 6 suggests that mode $2B^-$ will have even Fourier series components at $\beta=\{\ldots,-5\frac{\pi}{a},-1\frac{\pi}{a},3\frac{\pi}{a},\ldots\}$. Because waveguide modes are invariant under $\beta \rightarrow -\beta$, mode $2B^-$ will have even Fourier series components at $-\beta=\{\ldots,-5\frac{\pi}{a},-1\frac{\pi}{a},3\frac{\pi}{a},\ldots\}$ or $\beta=\{\ldots,5\frac{\pi}{a},1\frac{\pi}{a},-3\frac{\pi}{a},\ldots\}$. This suggests that when $\beta \rightarrow \pi/a$, modes $2A^+$ and $2B^-$ will have Fourier series peaks with even symmetry at the same points in Fourier space (insomuch as $+\beta$ can be considered the same point as $-\beta$ which for this disucssion it can be). A similar argument may be applied to the odd Fourier series components. Therefore, when $\beta \rightarrow \pi/a$ modes $2A^+$ and $2B^-$ have the *same* even-odd symmetry along the y direction. This is true for each pair of modes labeled with + and − signs.

Consider the third line of Eq. (6) which shows that the effect of operating with $\hat{g}$ on a representative field component is to multiply by $\pm e^{-i\beta a/2}$. Because modes are unchanged by taking $\pm\beta$, the implications of the relation on the third line of Eq. (6) are not altered by taking $\beta \rightarrow -\beta$: the result of operation by $\hat{g}$ may be written as $\pm e^{-i(\pm\beta)a/2}$. We still have only two eigenvalues characterized by + and −, but for each of those eigenvalues, the sign of the propagation constant may be changed without affecting this characterization. This modification does not affect the Fourier space symmetry properties previously discussed in this work. Consider the mode that transforms with a + sign under application of $\hat{g}$. When $\beta \rightarrow \pi/a$, its eigenvalue becomes $+e^{-i\pm\pi/a\times a/2}=+e^{-i\pm\pi/2}=\mp i$. Note that this is really a single eigenvalue whose duplicitous sign is a result of taking $\pm\beta$. Similarly, for the mode that transforms with a − sign under application of $\hat{g}$, one gets $-e^{-i\pm\pi/a\times a/2}=\pm i$. In these cases, the $\pm$ sign corresponds to the same mode (i.e. $\pm\beta$). Therefore, operation by $\hat{g}$ at $\beta=\pi/a$ is equivalent to $\beta \rightarrow -\beta$ suggesting the $\hat{g}$ operator has only a single unique eigenvalue at $\beta=\pi/a$.

TABLE III. Character table of C_{1h} point group.

$C_{1h}(m)$	E	σ_y
A	1	1
B	1	−1

Given that the modes labeled + and − evolve to modes with the same y direction even-odd symmetry at $\beta=\pi/a$ and that the eigenvalues of $\hat{g}$ switch from two distinct eigenvalues to effectively one eigenvalue, it is not surprising that the bandstructure exhibits pairwise degeneracy at $\beta=\pi/a$. In the next section we show that the pairwise degeneracy can be rigorously predicted using space group theory.

IV. SPACE GROUP ANALYSIS OF TWO-DIMENSIONAL PHOTONIC CRYSTAL WAVEGUIDES

A. Frieze groups: the space groups of two-dimensional photonic crystal waveguides

In this section we use group theory to characterize the modes in photonic crystal waveguides. The pairwise degeneracy at the Brillouin zone for type B waveguides will be predicted via nonsymmorphic space group analysis. Group theory[26] has been used in photonic crystal research to understand and classify both extended Bloch modes and localized defect modes.[27–30] The previous literature, however, focused on point groups. Point groups are subgroups of space groups and the theory of space groups allows for the classification of a broader class of photonic crystal lattice geometries. In this section, we examine the symmetry properties of two-dimensional photonic crystal waveguides in the context of space groups and focus on the nonsymmorphic space group of the type B waveguide.

Space groups,[31] consisting of point group operations and translation group operations, can be described by the Seitz operator $\{R|t\}$ defined by a point operation R followed by a translation t. Note that in this section, in order to simplify notation, a symmetry operator will no longer be denoted with a hat ($\hat{}$). The Seitz operator operates on an arbitrary position vector r as $\{R|t\}r=Rr+t$. For a Bravais lattice, its space group involves all the translations of the lattice vectors that are linear combinations of the primitive lattice vectors.

But this space group may also involve a translation (τ) smaller than a primitive lattice translation coupled with a rotation or reflection. These operations are known as "screw rotations" and "glide reflections." A space group is "nonsymmorphic" if it contains screw or glide operations. Otherwise it is "symmorphic." Furthermore, all the elements of a symmorphic space group can be written as the direct product (denoted by $\otimes$) of translation groups and point groups. This is not the case for nonsymmorphic space groups. A screw rotation, whose translation is parallel to the rotation axis, does not exist when the space dimension is lower than three. Glide reflection is the only "nonsymmorphic operation" in the two-dimensional space group.

Among the crystallographic space groups of three-dimensional lattices, there are 73 symmorphic groups and 157 nonsymmorphic groups. In the case of two-dimensional lattices, there are 13 symmorphic groups and four nonsymmorphic groups. These groups are often refered to as wallpaper groups, due to their likeness to a repeating wallpaper pattern on a two-dimensional wall or plane. The space group of two-dimensional patterns containing only one-dimensional translation is called the Frieze group. This is the space group of a two-dimensional photonic crystal waveguide. It has five symmorphic groups and two nonsymmorphic groups.

In Fig. 7, the total number of seven Frieze groups are labeled and illustrated using simple examples.[32] The symbols for the group starts with "F" as in Frieze. The number "1" and "2" refers to the rotation operator C_1 and C_2. "m" indicates the existence of a mirror operation and "g" means a glide operation. The space group of type A waveguide is F_{2mm} (symmorphic group) and the space group of type B waveguide is F_{2mg} (nonsymmorphic group).

In the following two subsections, we will analyze the type A and type B photonic crystal waveguides using the Frieze groups F_{2mm} and F_{2mg}. We choose to work on these two groups because they are the symmorphic and nonsymmorphic Frieze groups of the highest symmetry. The rest of the five Frieze groups can be constructed by removing one or

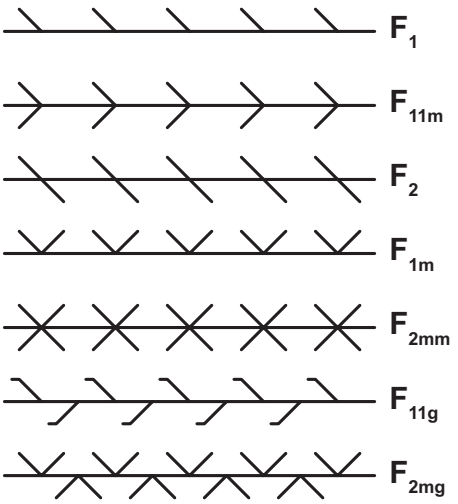

FIG. 7. The seven Frieze groups. (Ref. 32) F_{11g} and F_{2mg} are nonsymmorphic groups containing glide reflections. The rest are symmorphic.

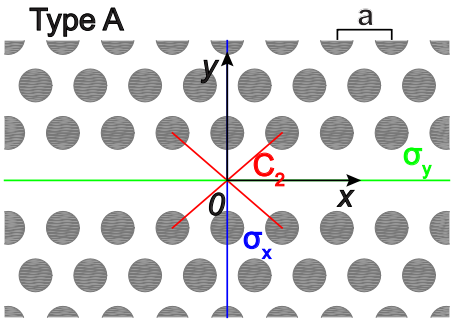

FIG. 8. (Color online) Illustration of a type A photonic crystal waveguide and its symmetry operations.

two symmetry operations from F_{2mm} or F_{2mg}. Note that these results can be applied to two-dimensional photonic crystal slab structures with top and bottom cladding layers so long as these cladding layers do not break the in-plane symmetry of the waveguide.

B. Symmorphic space group of type A photonic crystal waveguides

The symmorphic space group of the dielectric structure of the type A photonic crystal waveguide F_{2mm} is isomorphic to the direct product of a translation group and a point group ($T_{na} \otimes C_{2v}$). The translation group $T_{na}=\{E|na\}$ is Abelian and has only one-dimensional representations which are complex numbers. Therefore, we can always analyze the point groups alone for symmorphic space groups. In the Seitz operator, E is a unity operator, n is an arbitrary integer and a is the lattice constant introduced in Fig. 1 and illustrated in Fig. 8. The point group is $C_{2v}=(E, C_2, \sigma_x, \sigma_y)$ as illustrated in Fig. 8, where σ is the reflection operator.

The point group of wave vectors (k) (also known as the "little group") consists of point group elements that transform k into itself or an equivalent point that is connected by reciprocal lattice vectors. It is denoted as G^k and is a subgroup of the point group. In the case of the type A waveguide, G^k is a subgroup of C_{2v}. At the Brillouin zone center

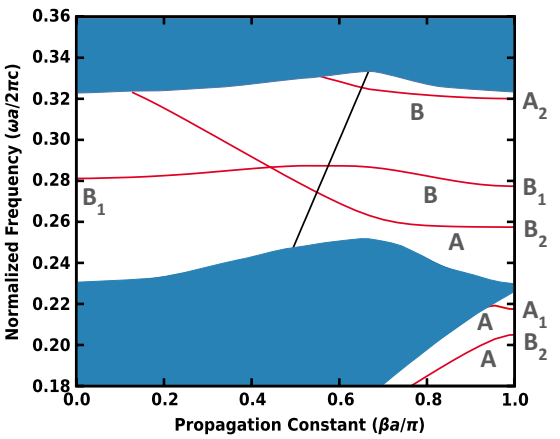

FIG. 9. (Color online) The dispersion diagram of the type A waveguide. The representations are assigned according to the H_z field component of the waveguide mode profiles.

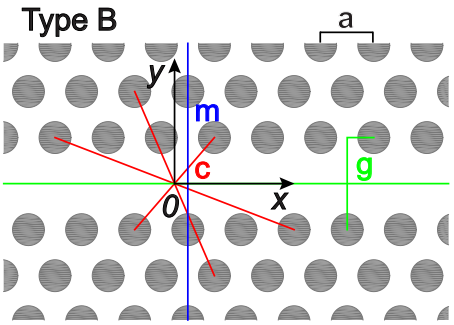

FIG. 10. (Color online) Illustration of a type B waveguide and its symmetry operators.

and edge, $G^{k=0}=G^{k=\pi/a}=C_{2v}$. For "general" k points inside the Brillouin zone, the point group is $G^{0<k<\pi/a}=C_{1h}=(E,\sigma_y)$. The character tables of the point groups C_{2v} and C_{1h} are shown in Tables II and III, respectively. Their compatibility relation is evident from the eigenvalues of the σ_y operation. The dispersion curves of the type A waveguide are assigned to the representations in the character tables in Fig. 9 according to the H_z field components of the waveguide modes. These eigenmodes are irreducible representations of the group.

Because all the representations of C_{2v} are one-dimensional, there is no degeneracy imposed by symmetry. The crossing of waveguide modes "A" and "B" in the middle of the TE band gap is accidental.

V. NONSYMMORPHIC SPACE GROUP OF TYPE B PHOTONIC CRYSTAL WAVEGUIDES

The symmetry operations of the type B waveguide are illustrated in Fig. 10. They include e, c, m, and g, where

$$e=\{E|0\},$$

$$c=\{C_2|0\},$$

$$m=\{\sigma_x|a/2\},$$

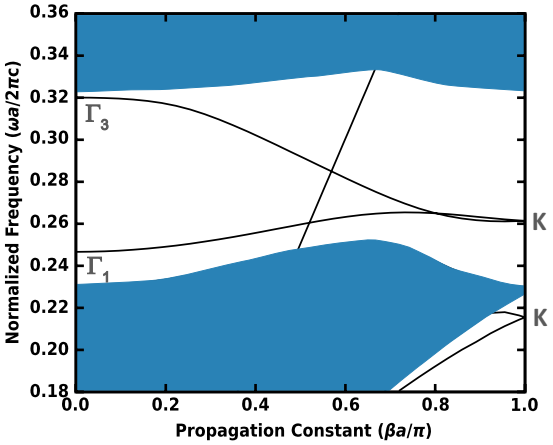

FIG. 11. (Color online) The dispersion diagram of the type B waveguide. The representations are assigned according to the H_z field component of the waveguide mode profiles.

TABLE IV. Character table of the factor group of $F^{k=0}_{2mg}/T_{na}$.

$F^{k=0}_{2mg}/T_{na}$	eT_{na}	cT_{na}	mT_{na}	gT_{na}
Γ_1	1	1	1	1
Γ_2	1	1	−1	−1
Γ_3	1	−1	1	−1
Γ_4	1	−1	−1	1

$$g=\{\sigma_y|a/2\}. \quad (8)$$

The coordinate origin is chosen at the center of the C_2 rotation, so it is quarter-lattice-constant shifted away from a lattice point along the x direction at the center of the defect region. The mirror operation σ_x is thus not with respect to the vertical line through the origin. The g operator is the glide reflection.

Being different from the type A case, these nontranslation operations (e,c,m,g) do not form a group due to the existence of the glide operation. For example consider g. Then $g^2=\{E|a\}$ becomes a pure translation which is not a member of the nontranslation elements just listed. Therefore, it is not possible to express the nonsymmorphic group as the direct product of a translation group and a point group. Furthermore, the translation group, $T_{na}=\{E|na\}$, has an infinite number of elements. Fortunately, it is an invariant subgroup (normal divisor), and we can divide it out. The resulting factor group can be analyzed with a finite number of elements and is homomorphic to the original space group.[33]

At $k=0$, the whole translation group $T_{na}=\{E|na\}$ is the normal divisor, since $e^{k\times na}=e^{0\times na}=1$. The factor group

$$F^{k=0}_{2mg}/T_{na}=(eT_{na},cT_{na},mT_{na},gT_{na})$$
$$=(\{E|na\},\{C_2|na\},\{\sigma_x|a/2+na\},\{\sigma_y|a/2+na\})$$

where the elements of the factor group are cosets of the normal divisor. This factor group is isomorphic to the point group C_{2v}, and the character table is listed in Table IV. The representations in Table IV are all one dimensional. Therefore one expects the type B waveguide bands to be nondegenerate at $k=0$.

At $k=\pi/a$, the translation group $T_{2na}=\{E|2na\}$ is the normal divisor, since $e^{k\times 2na}=e^{\pi/a\times 2na}=1$. Then the factor group $F_{2mg}/T_{2na}=(e',\bar{e}',c',\bar{c}',m',\bar{m}',g',\bar{g}')$.[34,35] It has eight elements and they are

$$e'=\{E|2na\},$$

$$\bar{e}'=\{E|a+2na\},$$

$$c'=\{C_2|2na\},$$

$$\bar{c}'=\{C_2|a+2na\},$$

$$m'=\{\sigma_x|a/2+2na\},$$

$$\bar{m}'=\{\sigma_x|a/2+a+2na\},$$

$$g'=\{\sigma_y|a/2+2na\},$$

TABLE V. Character table of the factor group of F_{2mg}/T_{2na}. The two-dimensional irreducible representation (K) is also shown in the unity matrix form.[36]

F_{2mg}/T_{2na}	e'	$\bar{e}'$	$c', \bar{c}'$	$m', \bar{m}'$	$g', \bar{g}'$
	1	1	1	1	1
	1	1	1	−1	−1
	1	1	−1	1	−1
	1	1	−1	−1	1
K	2	−2	0	0	0
	$\begin{pmatrix}1 & 0\\0 & 1\end{pmatrix}$	$\begin{pmatrix}-1 & 0\\0 & -1\end{pmatrix}$	$\begin{pmatrix}i & 0\\0 & -i\end{pmatrix}$	$\begin{pmatrix}0 & 1\\-1 & 0\end{pmatrix}$	$\begin{pmatrix}0 & i\\i & 0\end{pmatrix}$

$$\bar{g}' = \{\sigma_y | a/2 + a + 2na\}. \quad (9)$$

This factor group is isomorphic to the point group C_{4v} and its character is shown in Table V. There are four one-dimensional representations and one two-dimensional representation. For a Bloch wave representation at the Brillouin zone boundary ($k=\pi/a$), a one lattice vector translation $\{E|a\}$ changes the representation by a minus sign ($e^{k\times a} = e^{\pi/a\times a} = -1$). The only representation that changes the sign for the characters between $e' = \{E|2na\}$ and $\bar{e}' = \{E|a+2na\}$ is K which is two dimensional. K is then the only compatible representation at $k=\pi/a$.

Because K is a two-dimensional representation, the waveguide modes of a type B waveguide should be two-fold degenerate at the Brillouin zone boundary. This explains the double-degeneracy of all the type B waveguide dispersion bands at the Brillouin zone boundary. This "bands sticking together" effect is associated with the glide reflection symmetry that makes the space group nonsymmorphic.

The dispersion curves of the type B waveguide are assigned with representations from the character tables in Fig. 11, according to the H_z field components of the waveguide modes. For a general point in the Brillouin zone, none of the space symmetry operations leave the k vector invariant or shifted by a reciprocal lattice vector of the waveguide (other than translation by a). Therefore, the representation for a general point in the Brillouin zone is trivial (i.e. the identity representation) and not labeled.

The two-by-two unitary matrix irreducible representation of K is shown at the bottom of Table V. It is helpful in revealing the relation between the real-space field distributions of the two degenerate modes at the Brillouin zone boundary. It is apparent that the operators (m,m') and (g,g') transform one mode to the other with only an extra phase factor (-1 or i) while the dielectric structure remains the same after these operations. This implies they share the same frequency at the Brillouin zone boundary and are, thus, degenerate there.

VI. CONCLUSION

In this work, we have discussed the symmetry, Fourier space and space group properties of two-dimensional photonic crystal waveguides. It was shown that the modes of a type A waveguide can be characterized as even or odd along the y direction whereas the glide plane in a type B waveguide introduces more complicated symmetry properties. In particular, the modes of a type B waveguide decompose into spatial Fourier series components with alternating even and odd symmetry along the y direction. The theory of symmorphic and nonsymmorphic space groups was used to classify the modes of type A and type B waveguides. The results of the nonsymmorphic space group analysis predict the pairwise degeneracy at the Brillouin zone boundary of the type B waveguide. In addition to its general theoretical interest, this work is applicable to the design of photonic crystal waveguides for integrated photonics and slow light applications.

ACKNOWLEDGMENTS

This work was funded by the Defense Advanced Research Projects Agency (DARPA) under Contract No. F49620-02-1-0403. Computation for the work described in this paper was supported, in part, by the University of Southern California Center for High Performance Computing and Communications.

*mock1ap@cmich.edu

[1] O. Painter, R. K. Lee, A. Scherer, A. Yariv, J. D. O'Brien, P. D. Dapkus, and I. Kim, Science **284**, 1819 (1999).

[2] S. J. McNab, N. Moll, and Y. A. Vlasov, Opt. Express **11**, 2927 (2003).

[3] H.-G. Park, S.-H. Kim, S.-H. Kwon, Y.-G. Ju, H.-K. Yang, J.-H. Baek, S.-B. Kim, and Y.-H. Lee, Science **305**, 1444 (2004).

[4] A. Mock, L. Lu, E. H. Hwang, J. O'Brien, and P. D. Dapkus, IEEE J. Sel. Top. Quantum Electron. **15**, 892 (2009).

[5] L. Lu, A. Mock, T. Yang, M. H. Shih, E. H. Hwang, M. Bagheri, A. Stapleton, S. Farrell, J. D. O'Brien, and P. D. Dapkus, Appl. Phys. Lett. **94**, 111101 (2009).

[6] M. H. Shih, W. J. Kim, W. Wuang, J. R. Cao, H. Yukawa, S. J. Choi, J. D. O'Brien, and W. K. Marshall, Appl. Phys. Lett. **84**, 460 (2004).
[7] T. Baba, Nat. Photonics **2**, 465 (2008).
[8] H.-Y. Ryu, M. Notomi, and Y.-H. Lee, Appl. Phys. Lett. **83**, 4294 (2003).
[9] B.-S. Song, S. Noda, T. Asano, and Y. Akahane, Nature Mater. **4**, 207 (2005).
[10] M. Notomi, A. Shinya, K. Yamada, J.-i. Takahashi, C. Takahashi, and I. Yokohama, IEEE J. Quantum Electron. **38**, 736 (2002).
[11] K. Srinivasan and O. Painter, Opt. Express **10**, 670 (2002).
[12] T. Asano, B.-S. Song, and S. Noda, Opt. Express **14**, 1996 (2006).
[13] W. Kuang, W. J. Kim, A. Mock, and J. D. O'Brien, IEEE J. Sel. Top. Quantum Electron. **12**, 1183 (2006).
[14] M. H. Shih, W. Kuang, T. Yang, M. Bagheri, Z.-J. Wei, S.-J. Choi, L. Lu, J. D. O'Brien, and P. D. Dapkus, Photonics Technology Letters **18**, 535 (2006).
[15] H. Benisty, J. Appl. Phys. **79**, 7483 (1996).
[16] W. Kuang and J. O'Brien, Opt. Lett. **29**, 860 (2004).
[17] M. H. Shih, A. Mock, E. H. Hwang, W. Kuang, J. D. O'Brien, and P. D. Dapkus, Conference on Lasers and Electro-Optics Technical Digest, CMKK3 2006 (unpublished).
[18] A. Mock and J. D. O'Brien, IEEE J. Lightwave Technol. **28**, 1042 (2010).
[19] A. Chutinan, M. Okano, and S. Noda, Appl. Phys. Lett. **80**, 1698 (2002).
[20] T. Baba and D. Mori, J. Phys. D **40**, 2659 (2007).
[21] A. Taflove and S. C. Hagness, *Computational Electrodynamics* (Artech House, Massachusetts, 2000).
[22] W. Kuang, W. J. Kim, and J. D. O'Brien, J. Lightwave Technol. **25**, 2612 (2007).
[23] A. Mock and J. D. O'Brien, Opt. Quantum Electron. **40**, 1187 (2009).
[24] A. Mock, L. Lu, and J. D. O'Brien, Opt. Express **16**, 9391 (2008).
[25] A. V. Oppenheim, R. W. Schafer, and J. R. Buck, *Discrete-Time Signal Processing*, 2nd ed. (Prentice Hall, New Jersey, 1999).
[26] M. Tinkham, *Group Theory and Quantum Mechanics* (Dover Publications, Inc., New York, 1964).
[27] K. Sakoda, *Optical Properties of Photonic Crystals* (Springer, Germany, 2001).
[28] M. Okano and S. Noda, Phys. Rev. B **70**, 125105 (2004).
[29] W. Kuang, J. R. Cao, T. Yang, S.-J. Choi, P.-T. Lee, J. D. O'Brien, and P. D. Dapkus, J. Opt. Soc. Am. B **22**, 1092 (2005).
[30] S.-H. Kim and Y.-H. Lee, IEEE J. Quantum Electron. **39**, 1081 (2003).
[31] G. Burns and A. Glazer, *Space Groups for Solid State Scientists* (Academic Press, Inc., New York, 1990).
[32] R. Mirman, *Point Groups, Space Groups, Crystals, Molecules* (World Scientific, Singapore, 1999).
[33] C. Herring, J. Franklin Inst. **233**, 525 (1942).
[34] V. Heine, *Group Theory in Quantum Mechanics* (Pergamon Press, New York, 1960).
[35] L. M. Falicov, *Group Theory and Its Physical Applications* (The University of Chicago Press, Chicago, 1966).
[36] A. Cracknell, Thin Solid Films **21**, 107 (1974).